# Negative Ion Beams and Secondary Beams

M. Cavenago*[1], P. Veltri[2], E. Gazza[2], G. Serianni[2], P. Agostinetti[2]
[2]INFN/LNL, Laboratori Nazionali di Legnaro, [2]Consorzio RFX, Assoc. Euratom-ENEA sulla Fusione
* viale dell'Universita' n. 2, I-35020 Legnaro (PD) Italy, cavenago@lnl.infn.it

**Abstract:** The development of powerful negative ion sources requires precise and versatile simulation tools to predict the emittance of the extracted ion beams and the heat load on the electrodes (mainly due to primary electrons and secondary ions). A first tool is a determination of the plasma beam interface (a thin sheath, that is a layer of charged plasma, usually called also meniscus in accelerator literature) which is accomplished by a set of macro (named Bypo17), based in the Comsol Multiphysics environment. Space charge both of the negative ions and of the coextracted electrons is taken into account, as well as a magnetic field $B_y(z)$ perpendicular to the beam extraction axis $z$. Mesh size is finer than the Debye length $\lambda_D$ in the meniscus. Notwithstanding the strong nonlinearities involved, a proper sequence of solver settings allows convergence to solution. Also a simple gas pressure model is included. A second tool consist in a database of atomic collision reactions that produce secondary ions, easily readable by Comsol Multiphysics. A third tool compute the secondary particle trajectories and the resulting heat load. As a final tool, the electrode temperature rise is simulated both with 2D an 3D Comsol Multiphysics models.

**Keywords:** ion beams, secondary beam, heat load

## 1 Introduction

Neutral Beam Injectors (NBI) envisioned for tokamaks (the ITER project and beyond) require development of negative ion sources (up to ion energies of 1 or 2 MeV) with carefully reduced beam divergence [1, 2]. A multiphysics approach is requested for studying most of physical and engineering issues involved[3, 4], as described partly in this paper.

Negative ions are separated by a magnetic field from the co-extracted electrons, which are dumped against accelerator electrodes. Thanks to multiaperture gridded electrodes, many beamlets are extracted (from 2 in test sources up to 1280 in a final device), so that a total of 40 A beam may be produced. A typical accelerator scheme is shown in fig 1; we have several intermediate elecrodes, from 3 (in test sources) up to 7. Current density at the source is $j_o = 240$ A/m$^2$ for $D^-$ sources, considered equivalent to $j_{H^-} = 340$ A/m$^2$ for $H^-$ test sources. Due to the gas flowing from the source (filling pressure 0.3 Pa), the gas pressure in the accelerator is rather large, with a 0.001 to 0.05 Pa pressure inside the beam tubes; in reference design, up to a 15 % beam loss is considered tolerable.

The thermal load on electrode is not uniform: even if secondary particles are generated with random coordinates, they are subjected to strongly not uniform fields, with possible focusing action. The load from primary electrons is even more focused, with peaks of the 10 MW/m$^2$ order. Cooling channels are placed as near to the hot area as it is possible in manufacturing; copper based alloys are used for the electrodes; even so, significant temperature gradients are found.

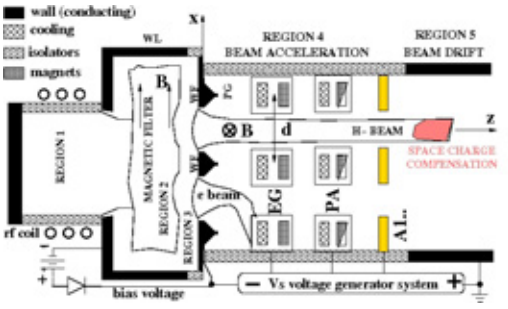


Figure 1: A scheme (not to scale) of the ion source and the accelerator: region 1 is the driver plasma, 2 is the filter, and 3 the plasma sheath (size greatly magnified); in the accelerator region 4, EG is the extraction grid, PA is the preacceleration grid and A1.. represents additional electrodes (if any). In some case PA is also grounded and called GG (grounded grid)

It is generally believed that modeling of a negative ion accelerator can be broken into several 2D or 3D modeling tasks: 1) magnetic field simulation; 2) gas flow; 3) self-consistent solution, based on precise finite element solvers, of primary beam extraction for one or two beamlet sections, with periodic lateral boundary conditions to simulate the whole grid; 4) Monte Carlo style simulations of the secondary particles generation, which may be very time consuming (even for one or two beamlets); 5) simulation of electrode heating and stresses; 6) a global simulation of repulsion between beamlets, where they are not shielded by electrodes.

Electric field must be obtained from a nonlinear Poisson equation, with a space charge density to be computed from particle motion; inside plasma space charge becomes negligible within lengths comparable to the Debye length, equal to 0.014 mm for a typical density plasma (corresponding to an extracted current of 340 A/m$^2$).

# 2 Governing equations

Near extraction, we assume that charged particles have the same temperature $T$, for which we use energy units; for example $T =$ 1 eV. Experimentally the extracted $H^-$ and electron currents are of the same order, so we introduce the ratio $R_j = j_e/j_{H^-}$ between the emitted electron flow and the $H^-$ one as a parameter in our simulation; for example $R_j = 1$. The simple estimate of the extracted flow $j_{H^-} = 0.6 c_s N_H^-$ where $c_s = \sqrt{T/m_H}$ is the Bohm speed shows that the ion density in the plasma just facing the extraction is $N_{H^-} = 3.1 \times 10^{17}$ m$^{-3}$ for $j_{H^-} = 340$ A/m$^2$, while the electron density estimated from $J_e = 0.6 R_m c_s N_e$ is lower; here $R_m = (m_H/m_e)^{1/2}$. Let $N_0$ the sum of negative particle densities taken as another input parameter; for example $N_0 = 3.2 \times 10^{17}$ m$^{-3}$.

We find convenient to introduce the scaled potential $u = -e\phi/T$, where $\phi$ is the electrostatic potential, and the scaled densities $n_i = N_i/N_0$. The Poisson equation is

$$\lambda_D^2 \triangle u = n_{H^+} - n_e - n_{H^-} \qquad (1)$$

with the Debye length $\lambda_D = (\epsilon_0 T/e^2 N_0)^{1/2}$. We also use scaled velocities $\mathbf{v} = \mathbf{v}/c_s$ and flow density $j_i = J_i/(c_s N_0)$ and introduce a flow modulus $j_\Sigma = \int \mathrm{d}^3 v \, |v| f$ where $f$ is the phase space density.

The density of positive ions (which are reflected by extraction meniscus) can be obtained from diffusion equations; in the limit of zero proton current, we retrieve the well known Maxwellian distribution

$$n_{H^+} = k_0 \exp(u - u_{cr}) \qquad (2)$$

where $k_0 = 1$ and $u_{cr}$ is a sort of plasma potential. Density of negative ions is

$$n_{H^-}(z,x) = j_\Sigma^{H^-}(z,x)/\sqrt{t_H - 2u + 2u_{cr}} \qquad (3)$$

with $t_H \cong 0.5$ a small parameter; similarly for electrons. Actually $j_\Sigma$ is calculated with integration and interpolation from ray tracing results[5, 6]; inside plasma, collisions make $j_\Sigma$ uniform.

In Bypo we restrict to a 2D geometry $zx$ with a perpendicular $B_y$ magnetic field; the scaled magnetic field is $b = B_y/B_0$, where $B_0$ is a fixed reference level, for example $B_0 = 20$ G. The ion ray tracing equations are

$$\begin{aligned} d_\ell z &= i_p(u_{,z} + v_x b/L) \\ d_\ell x &= i_p(u_{,x} - v_z b/L) \end{aligned} \qquad (4)$$

where $d_\ell a = da/d\ell$ is the total derivative, $\ell = c_s t$ and $L = m_H c_s/eB_0$ is the ion Larmor gyroradius and $i_p$ is the charge state. Similarly for electrons; but the Larmor radius $L_e = L/R_m$ becomes smaller than the extraction radius $r_h$; for example $L_e = 1.2$ mm and $r_h = 7$ mm.

## 2.1 Solution methods

It should pointed out that the plasma-negative ion sheath is a much more complicate problem than it is usally perceived (especially in existing codes), even in a 2D geometry. The system of eq. (1-3) with a fixed $j_\Sigma$ is in the form of a nonlinear PDE problem suited for Comsol Multiphysics (CM) solution; anyway it implies two scale lengths ($\lambda_\mathrm{D}$ and $r_h$)[7], so that its numerical solution is extremely challenging, and requires a extremely refined mesh; the large number of degrees of freedom makes nonlinear solver convergence more difficult[8], unless a correct and tested initialization procedure is used. Actually initialization procedures are being constantly improved in Bypo versions. Up to Bypo17, the reduction of the actual

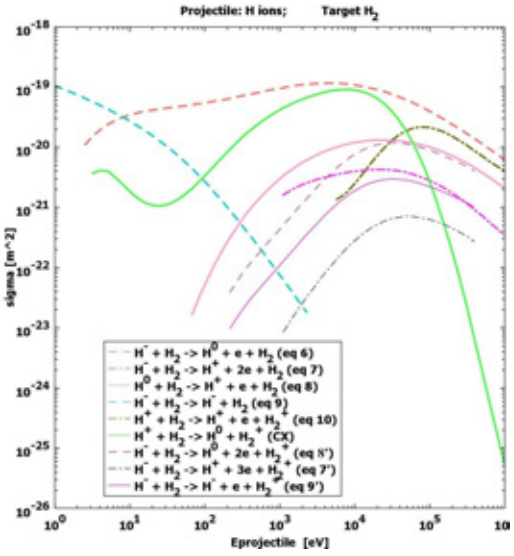

Figure 2: Cross sections of H ions against $H_2$

plasma density and a correspondent scaling of other input conditions was necessary for a robust calculation. This reduction is no longer necessary from Bypo18, which handles the full plasma density.

A less important, but more obvious remark is the need of iterative ray tracing[9]: after a solution for $u$ is found for a given $j_\Sigma$, ray tracing (using Comsol postprocessing) is repeated, so that a new value for $j_\Sigma$ is found. Typically from 4 to 9 iterations are enough.

Another important point[5] is that ray density is refined where the ray divergence is large; elsewhe rays can be interpolated. This allow to speed up the computation, or in more accurate words, it allows to satisfy the condition of one ray per mesh unit without a prohibitive computational load.

## 2.2 Electrode heating

Since an accurate description of the 2D geometry of the electrode system is represented in Bypo, it is natural to use it for related simulations: 1) gas flow; 2) thermal analysis (both 2D and 3D). The gas flow is computed in the initialization step of Bypo with an empirical model[4].

Some preliminary thermal analysis is here discussed. In consideration of the periodic structure of the electrodes, only one cell was studied. The temperature was fixed to $75^0$ C at the cooling pipe surface, from global consideration, while the heat load on the electrode, coming from primary and secondary beams, may be at first based on the 2D Bypo results. Also some preliminary heat load data from other codes was used for a comparison. Copper conductivity was fixed to 400 W / m K as found in the CM Material Library.

# 3 Beam-gas collisions

Database of known collision reactions of hydrogen molecules and ions is large and constantly upgraded[10, 11, 12]; anyway, still consultation of databases has to be completed with simple physical ideas to include all relevant processes. We converted many of these reaction data in structured variables, readable by CM; see Fig. 2.

A large variety of atomic collisions is possible[10, 13, 14, 15] at low energy inside plasma. Due to the rapid acceleration of the ions after they pass the extraction meniscus, only collisions with beam energy $E_b > E_1 \cong 1$ keV need to be considered in the secondary production. This consideration practically corresponds to restrict beam-gas collisions to the $z > 0$ domain (the accelerator tube), which helps to avoid unnecessary calculations. Here the gas target is taken at rest. The number of collision $X$ with gas (per unit time) on an element $\mathrm{d}s$ of a primary ray can be written $\mathrm{d}\,N = J_r \sigma_X(E_b) N_g \,\mathrm{d}s$ where $J_r$ is the particle flow associated with that ray, $N_g$ is the gas density and $\sigma_X(E_b)$ is the cross section; equivalently, using Bypo variables, the rate density $R_X$ of reaction $X$ is

$$\mathrm{d}^3N/\mathrm{d}^3x\ \mathrm{d}t \equiv R_X = [N_0 c_s] j_\Sigma \sigma_X(E_b) N_g \tag{5}$$

It is also important to model the reaction product velocity, which is usually determined by simple rules (when differential cross sections are not readily available); we often find useful the distinction of slow outputs from faster outputs, which maintain a significant part of the projectile speed (sometime underlined or overlined). It is convenient to assign to slow outputs a small energy $E_c$, to simplify tracing and space charge calculation.

The electron detachment reactions are

$$\underline{H}^- + H_2 \rightarrow \underline{H}^0 + \underline{e} + H_2 \tag{6}$$

$$\underline{H}^- + H_2 \rightarrow \underline{H}^+ + 2\underline{e} + H_2 \tag{7}$$

$$\underline{H}^0 + H_2 \rightarrow \underline{H}^+ + \underline{e} + H_2 \tag{8}$$

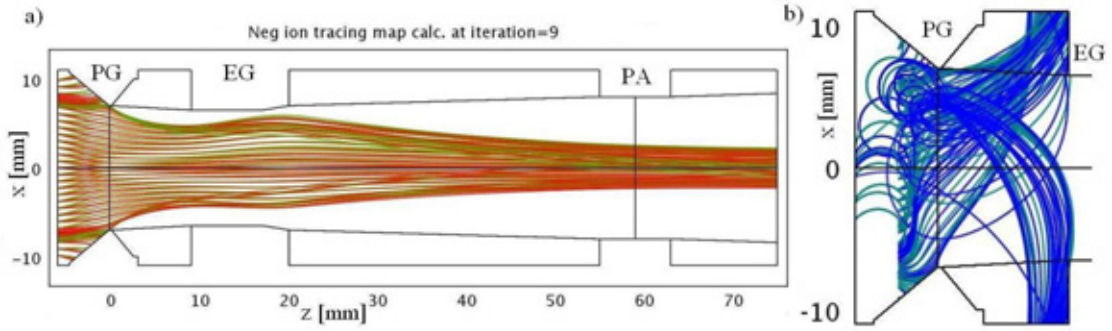


Figure 3: Panel a) Negative ion (red and green tones) acceleration between electrodes PG, EG and PA, with $R_j = 1$; b) a zoom of electron orbits (blue and green tones). Magnetic field is perpendicular to geometry

where the fast neutral projectile of eq. 8 is produced in eq. 6. In the case of elastic scattering

$$\underline{H}^- + H_2 \rightarrow \underline{H}^- + H_2 \qquad (9)$$

the cross section has the meaning of momentum transfer cross section, and is very small (less than $6 \times 10^{-22}$ m$^2$ ) for $E > 1$ keV. For all these collisions eqs (6-9) we can consider partner reactions in which the $H_2$ is fragmented (indicated with a $'$ mark) and similar (indicated with a $''$ mark). For example we have eq (8)$''$ where a fast $H^0$ breaks $H_2$ into $H_2^+$ and $e$; its cross section is greater than the proton impact ionization

$$\underline{H}^+ + H_2 \rightarrow \underline{H}^+ + e + H_2^+ \qquad (10)$$

at energy $E_b < 30$ keV, because the electron contained in the fast hydrogen atom participates to the collision also with its orbital speed. This fact leads also to consider reaction (9)' in secondary particle calculations[12]; we also consider (6)' ; some critical assessed cross sections are shown in fig 2.

We note that above reactions have the following major effects (confirmed by the simulations): 1) a loss of beam intensity (and space charge); the survival fraction is

$$F_s(z) = \exp\left\{-\int_0^z \mathrm{d}z\, \sigma(E_b)\, N_g(z)\right\} \qquad (11)$$

where $E_b = -Tu(z)$ and the cross section $\sigma$ is the sum of eqs. (6), (7) and partner reactions; 2) the production of electrons inside the $H^-$ beam, whose contribution to the space charge is much less than the one of the removed $H^-$, since electrons are rapidly accelerated; moreover they are soon deflected out of the beam; 3) the production of positive ions, which may be accelerated backward (toward a previous electrode or the source).

In the drifting beam region, where electrical field is low, the produced electron and positive ions are not swept away immediately, but may accumulate a significant space charge, which in turn may modify $u(z, x)$. This effect, named compensation of the beam space charge, is well known and somewhat approximated by 1D models[16], predicting a compensation ratio $R_{sc}$ for long uniform beams ( typically $R_{sc}$ ranges from 0.995 to 1.02 depending on pressure). In an empirical 2D model, the additional density of positive ions mostly $H_2^+$ may be written

$$n_p = n_{sc}\Theta(u_{,x} + v_1)\exp((u - u_{sc})/t_{sc}) \qquad (12)$$

with the parameters $n_{sc} = R_{sc} n_{H^-}(z_h, 0)$ and $t_{sc} = T_{sc}/T$, where the local ion temperature is $T_{sc}$ and the beam potential is $u_{sc} = u(z_h, 0)$; here $\Theta$ is the Heaviside function, delimiting the after-acceleration region, and $v_1 = 1$ V/m is a small field. In our example $R_{sc} = 0.997$ and $t_{sc} = 0.8$. Such a model is included from Bypo17 as well as eq. 11 to obtain a better $u(z)$ estimate.

# 4 Beam simulations

A selfconsistent simulation with a geometry similar to the SPIDER test source, formerly known as ISTF[17] is shown in fig. 3: the magnetic field profile (shown in fig 4) was just the minimal needed to ensure that primary electrons do not surpass the EG lower $z$ face. Note the electron orbits in the plasma

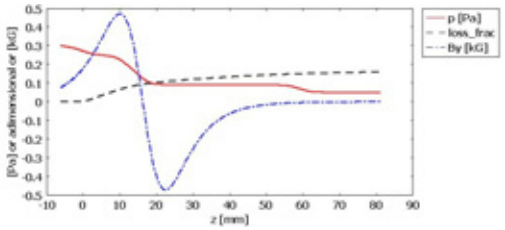


Figure 4: Profiles of the assumed magnetic field $B_y$, of the computed pressure $p$ and loss fraction $1 - F_s$

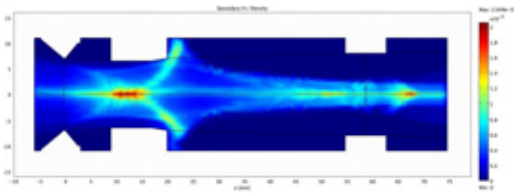

Figure 5: $H^+$ secondary beam density, which is higher where the ions decelerate and turn back towards the ion source. At production point, $H^+$ maintains quite all the parent $H^-$ velocity.

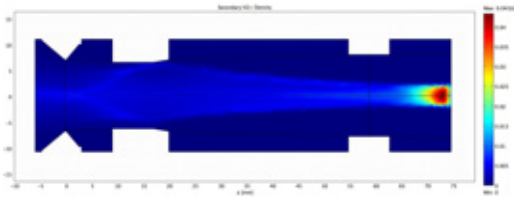

Figure 6: $H_2^+$ secondary beam density. These ions comes from ionization of the gas and thus have a small initial velocity.

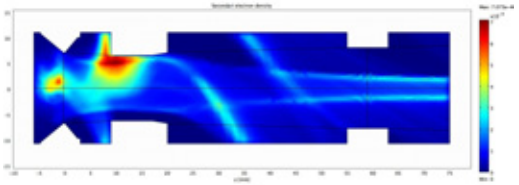

Figure 7: Secondary electrons density is low, due to their high velocity, but they still gives a small contribution to the heating of the EG.

before extraction. The magnetic field produces an appreciable deviation of the ion beam, which is subsequently steered in the EG to GG gap; to further straighten out the beam, we can consider to include opposite polarity magnets in the GG.

### 4.1 Secondary Beams

Results from secondary beam simulations are shown from Fig 5 to 8. Trajectories where computed with same CM postprocessor routine (`postplot`) and settings used in Bypo. Note the secondary particle space charge is generally much smaller than the primary ion one, except for the beam drift region.

In detail, the $H_2^+$ space charge shows the expected charge compensation at the drift tube, and agrees qualitatively with the eq 12 model.

## 5 Thermal simulations

The total power load computed by Bypo on the EG is shown in Fig. 9 as a function of $x$. In 2D thermal simulations, the temperature rise in the copper is limited to 10 K for a 1 mm wall thickness (Fig. 10).

For comparison fig. 9 also shows the heat load $P_E(x, y)$ computed by the Montecarlo code EAMCC[12], in the $y = 0$ section. In our 3D thermal simulations, we can either use $P_E(x, y)$, see Figs. 11-12, or extrapolate the Bypo heat load $P_B(x)$ in the $y$ direction as

$$\begin{aligned} P_b(x,y) &= \tfrac{1}{2}(1+\cos\vartheta)P_B(r) \\ &+ \tfrac{1}{2}(1-\cos\vartheta)P_B(-r) \quad (13) \end{aligned}$$

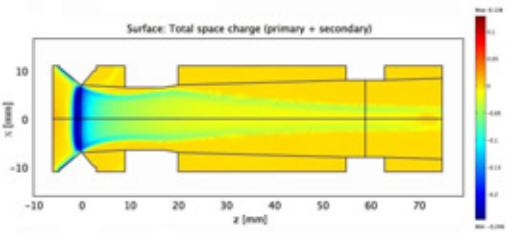


Figure 8: Sum of space charge of primary and secondary beams

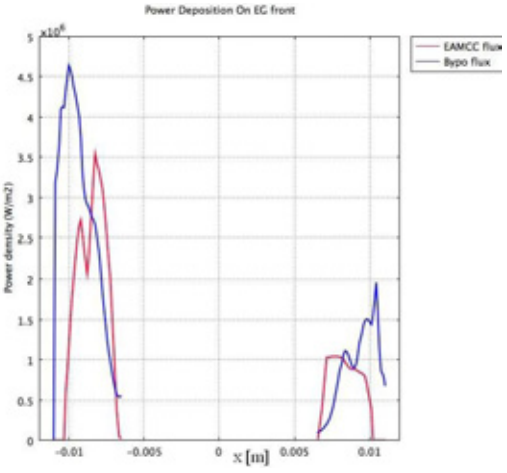


Figure 9: Heat loads comparison

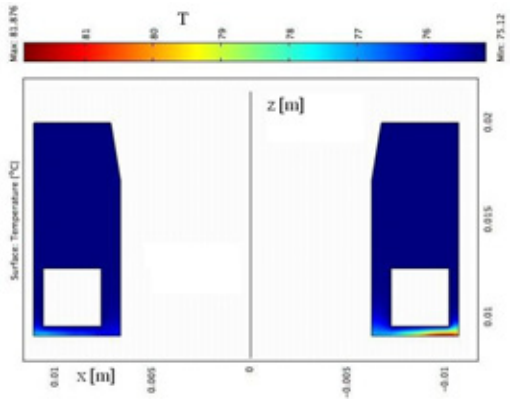


Figure 10: Extraction grid (EG) temperature in a 2D model

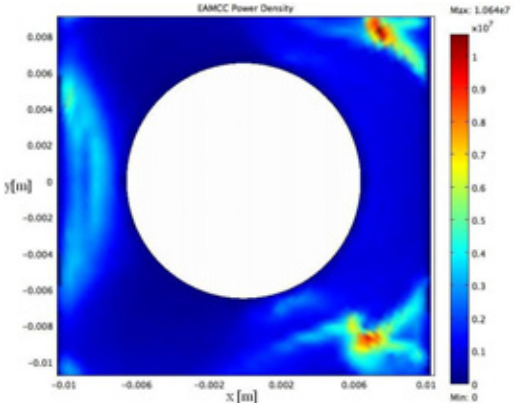


Figure 11: Heat load $P_E$ from Ref [12] code

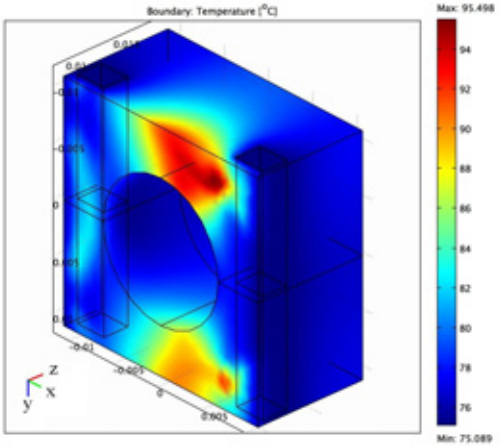


Figure 12: Extraction grid temperature in a 3D model with $P_E$

with $r, \vartheta$ polar coordinates. In the average, power loads from Bypo and EAMCC show a good agreement: from 2D boundary integration and multiplying for cell height, Bypo finds a power load of 435 W due to primary electrons and 8.6 W due to secondary electrons. EAMCC finds 450 W and 13 W, respectively.

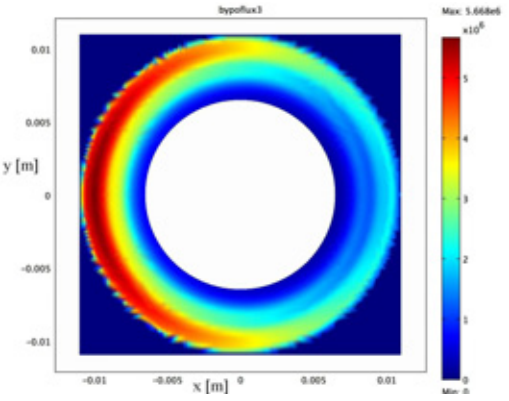


Figure 13: Heat load $P_b$ on the EG lower $z$ face extrapolated from Bypo

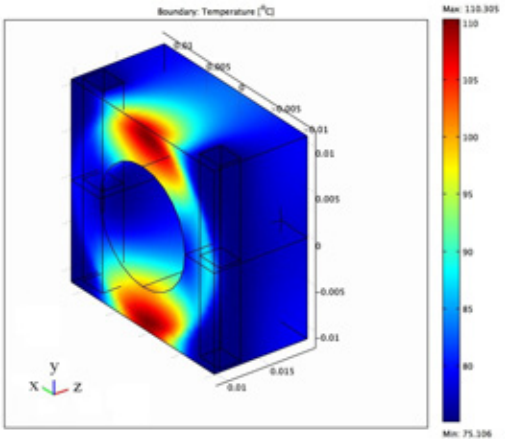


Figure 14: Extraction grid (EG) temperature in a 3D model with heat load $P_b$

The Bypo case Figs. 13-14 shows that temperature maximum is not at the load maximum, but moves in less cooled region. This is also evident with the EAMCC heat load.

# References

[1] H. P. L. de Esch, R. S. Hemsworth, and P. Massmann, SINGAP: The European concept for negative ion acceleration in the ITER neutral injectors, Rev. Sci. Instrum., **73**, pp1045-1047 (2002)

[2] T. Inoue et al., "Design of neutral beam system for ITER-FEAT", Fus. Eng. and Design 56-57 (2001) 517-521

[3] P. Agostinetti et al., "Design of a low voltage, high current extraction system for the ITER Ion Source" , in *Negative Ions Beams and Sources, 1st Int. Symposium*, AIP CP **1097**, (ed. E. Surrey, A. Simonin, AIP, Melville, 2009), p. 325

[4] M. Cavenago et al., "Development of Small Multiaperture Negative Ion Beam Sources" , ibidem, p 149.

[5] M. Cavenago, P. Veltri, F. Sattin, G. Serianni, V. Antoni, *IEEE Trans. on Plasma Science*, **36**, pp 1581-1588 (2008)

[6] M. Cavenago, P. Veltri, N. Pilan, P. Antonini, Simulations of Negative Ion Beams and Sources, in Comsol 2008 User Conference, CD-ROM (2008)

[7] A. Caruso, A.Cavaliere, *Nuovo Cim.*, **26**, 1389 (1962)

[8] M.Cavenago, "Structures of Charge Sheaths and Transition Layers in Ion Sources", in "Collective Phenomena in Macroscopic Systems " (eds. G Bertin, R Pozzoli, M Rom , K R Sreenivasan, World Scientific, Singapore), pp 225-230 (2007)

[9] J. H. Whealton et al. , *J. Appl. Phys.*, **64**, 6210(1988)

[10] R. K. Janev, D. Reiter, and U. Samm, Collision processes in low-temperature hydrogen plasmas, Tech. Rep. Jul-4105, Forschungszentrum Julich (2003)

[11] `http://www-amdis.iaea.org/ALADDIN` and links

[12] G. Fubiani, H. P. L. de Esch, A. Simonin, R. Hemsworth, Phys. Rev. ST-AB, **11**, 014202 (2008)

[13] J. Brcka, Modeling Remote H2 Plasma in Semiconductor Processing Tool, Proceedings of the COMSOL Users Conference 2006 Boston

[14] G. J. M. Hagelaar, J.-P. Boeuf and A. Simonin, "Modeling of an Inductive Negative Ion Source for Neutral Beam Injection", AIP Conf. Proc. **993**, 55 (2008)

[15] S. Kolev et al, "Magnetic filter operation in hydrogen plasmas", Plasma Phys. and Controlled Fusion, **49**, pp. 1349-1369 (2007)

[16] A. T. Holmes, *Beam Transport*, in *The Physics and Technology of Ion Sources*, (ed. I.G. Brown), J. Wiley, NY, 1989

[17] P. Agostinetti, S. Dal Bello, M. Dalla Palma, P. Zaccaria. "Thermomechanical design of the SINGAP accelerator grids for ITER NB Injectors", Fusion Eng. Des. **82** (2007) 860-866.